



Rethinking Orientation Estimation with Smartphone-equipped Ultra-wideband Chips

Hao Zhou^{1†}, Kuang Yuan², Mahanth Gowda¹, Lili Qiu^{3,4}, Jie Xiong^{3,5}

¹The Pennsylvania State University, ²Carnegie Mellon University, ³Microsoft Research Asia,

⁴University of Texas at Austin, ⁵University of Massachusetts Amherst

Abstract

While localization has gained a tremendous amount of attention from both academia and industry, much less attention has been paid to equally important orientation estimation. Traditional orientation estimation systems relying on gyroscopes suffer from cumulative errors. In this paper, we propose *UWBOrrient*, the first fine-grained orientation estimation system utilizing ultra-wideband (UWB) modules embedded in smartphones. The proposed system presents an alternative solution that is more accurate than gyroscope estimates and free of error accumulation. We propose to fuse UWB estimates with gyroscope estimates to address the challenge associated with UWB estimation alone and further improve the estimation accuracy. *UWBOrrient* decreases the estimation error from the state-of-the-art 7.6° to 2.7° while maintaining a low latency (20 ms) and low energy consumption (40 mWh). Comprehensive experiments with both iPhone and Android smartphones demonstrate the effectiveness of the proposed system under various conditions including natural motion, dynamic multipath and NLoS. Two real-world applications, i.e., head orientation tracking and 3D reconstruction are employed to showcase the practicality of *UWBOrrient*.

CCS Concepts

- Human-centered computing → Ubiquitous and mobile devices.

[†]This research was conducted during an internship at Microsoft Research Asia.

Keywords

Orientation estimation, Smartphone-based ultra-wideband sensing

ACM Reference Format:

Hao Zhou^{1†}, Kuang Yuan², Mahanth Gowda¹, Lili Qiu^{3,4}, Jie Xiong^{3,5}. 2024. Rethinking Orientation Estimation with Smartphone-equipped Ultra-wideband Chips. In *The 30th Annual International Conference on Mobile Computing and Networking (ACM MobiCom '24)*, November 18–22, 2024, Washington D.C., DC, USA. ACM, New York, NY, USA, 15 pages. <https://doi.org/10.1145/3636534.3690677>

1 Introduction

Orientation, which defines how an object or individual is facing in the environment plays a critical role in applications such as mobile gaming, VR (virtual reality), AR (Augmented reality), robotics, and 3D reconstruction. Unfortunately, orientation is often overshadowed by the emphasis on localization [10, 13, 14, 29, 32, 47, 52, 53]. In robotics [15, 43], while localization allows a robot to know where it is, orientation ensures the robot moves in the appropriate direction for tasks like navigation, industrial assembly, and interaction with humans or other robots. In VR/AR [30, 50], orientation is the key to provide users with an immersive experience, as understanding the orientation of a device, such as a smartphone or a dedicated VR headset, enables responsive and adaptive interactions. In the last two decades, we have seen a large amount of research on localization but much less research on orientation estimation.

Prior Arts. Traditional orientation estimation systems rely on an inertial gyroscope. Gyroscopes measure the instant angular velocity of the device and the device orientation can then be estimated by integrating the angular velocity over time. However, this method yields cumulative errors [37, 40]. While multiple solutions were proposed [41, 61], they are susceptible to magnetic interference. On the other hand, vision-based orientation estimation systems analyze visual data to determine the orientation of objects. However, lighting requirements, high power consumption, and occlusions pose challenges for vision-based orientation estimation solutions [2, 33].



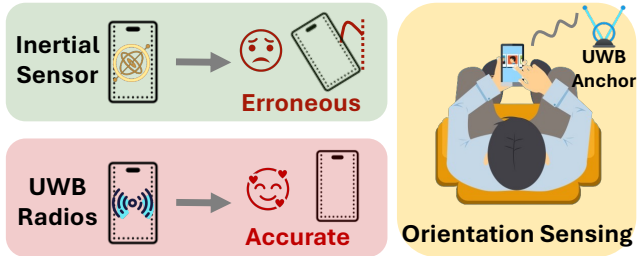


Figure 1: In contrast to inertial sensor-based solutions, *UWB* Orient leverages the Ultra-wideband (UWB) modules embedded in consumer-level electronics such as smartphones to achieve accurate orientation sensing.

New Opportunity. In this paper, we leverage an exciting new opportunity, i.e., consumer-level electronics such as smartphones and smartwatches are now equipped with Ultra-Wideband (UWB) chips for orientation estimation. UWB chip has been a default component in iPhones since 2019 [5]. Apple devices such as Apple Watch, HomePod mini, and AirTag are now all equipped with UWB chips. Other manufacturers such as Samsung, Google, and Xiaomi [36, 39] also include UWB chips in their products including Samsung S21 Ultra, Google Pixel Pro, Xiaomi MIX 4, Xiaomi smart speaker, and Mi TV. BMW [9] embeds UWB chips in their car keys. While the UWB module in these devices is still utilized for ranging to support applications such as FindMy [4], and keyless car entry [9], we propose to leverage UWB module embedded in smartphones for fine-grained device orientation estimation for the first time. We show that UWB-based orientation estimation exhibits unique advantages such as resilient against cumulative error and magnetic interference. Owing to the large bandwidth of UWB (e.g., 1 GHz), the effect of multipath interference is also significantly mitigated.

Challenges. Although UWB offers unique advantages, multiple challenges need to be addressed before we can make UWB-based orientation estimation work.

Challenge 1: Raw UWB readings cannot be obtained from smartphones. UWB-based sensing/tracking has been demonstrated using commodity UWB chips such as Qorvo EVK1000 and XeThru SLMX4. These chips can report raw UWB readings, i.e., signal amplitude and phase which are critical for sensing. However, although UWB chips are embedded in iPhone and Google Pixel phones, the low-level UWB signal amplitude and phase information is not available and the UWB API only reports high-level information such as distance [54]. This high-level information can be used for ranging but is too coarse for fine-grained orientation estimation.

In this paper, we leverage another piece of high-level information reported by smartphones (i.e., signal incident angle information) to achieve fine-grained device orientation estimation. Owing to the wide bandwidth, LoS path and reflections can usually be separated in different range bins and the accuracy of the reported angle information is surprisingly high based on our measurements.¹ This fine-grained angle information presents us with a unique opportunity to achieve highly accurate device orientation estimation. What is more exciting is that smartphones such as iPhone can report both azimuth and elevation angle readings and we can leverage them to achieve not just 2D but 3D orientation estimation.

Challenge 2: Rotation usually occurs together with translational motions. In practical scenarios such as VR/AR, pure rotational motion is rare and rotation is usually mixed with translational motions (e.g., users face to various directions while walking around). Unfortunately, when we leverage UWB-reported angle for orientation estimation, both rotational and translational motions can cause the angle to vary, confusing orientation estimation.

To address the challenge brought by the translational motion, we propose to involve gyroscopes which are available in almost all smartphones in our system. This design is motivated by two observations. First, although gyroscope-based orientation estimation has large cumulative errors over a long interval, the accuracy within a short duration (e.g., a few seconds) is still high. Second, while UWB-based angle measurements are affected by both rotational motion and translational motion, gyroscope measurements contain only rotational motion. Thus, gyroscope measurements can be used as a reference to identify UWB-reported angles that are interfered by translational motion.

Challenge 3: Traditionally, the fusion of UWB and inertial measurements focused on localization, in which the distance information was leveraged. It remains unknown how to fuse UWB estimates with inertial measurements for orientation estimation.

Based on whether the UWB estimates are interfered, we design a fusion scheme that dynamically fuses both modalities for accurate orientation estimation. Specifically, when UWB estimates are not interfered, the design is motivated by the observation that while the *rotation angle* of UWB estimates is more accurate than that of gyroscope estimates, the *rotation axis* exhibits a relatively larger error especially when the amount of rotation is small. Thus, we fuse UWB estimates with gyroscope estimates for improvement. When UWB estimates are

¹A median error below 3° can be achieved using one pair of iPhones.

interfered, we replace them with gyroscope estimates which are relatively accurate in a short period. In an extreme case of long-time interfered UWB angle estimates, the gyroscope estimates are also not accurate due to cumulative errors. In this case, we leverage the unaffected UWB distance estimates to correct the cumulative error of gyroscope estimates for orientation estimation.

Overview. By addressing these challenges, we propose *UWB Orient*, the first orientation estimation system based on UWB module in consumer-level electronics such as smartphones.

We demonstrate the effectiveness of *UWB Orient* on both iPhone and Android smartphones including Samsung and Google Pixel phones. The achieved median orientation error (2.7°) is significantly smaller compared to prior works (e.g., 7.6° for MUSE [41]). We also conducted extensive experiments to verify the effectiveness of *UWB Orient* in environments with rich dynamic multipath. *UWB Orient* is shown to be robust against dynamic multipath with a median error of 3.2° which is just slightly higher than that achieved without multipath. Other advantages of *UWB Orient* include only a single anchor is required. Note that *UWB Orient* has no requirement on the anchor placement such as location and orientation, and commonly seen devices such as AirTags, iPhones, and Samsung phones can be used as anchors without any modifications. *UWB Orient* is further applied to realize two real-world applications, i.e., head orientation tracking that is critical in VR/AR, and 3D reconstruction that reconstructs a target accurately with images taken from various orientations. The main contributions are summarized as follows.

- We employ the UWB module embedded in smartphones for ranging to realize fine-grained orientation estimation for the first time. Different from conventional UWB sensing which relies on raw UWB amplitude and phase readings, the proposed system utilizes the high-level UWB information available on smartphones to make fine-grained orientation estimation happen.
- Through deeply understanding the complementary characteristics between UWB and gyroscope, we propose to fuse information from UWB and gyroscope to deal with one practical challenge encountered, i.e., rotation is usually mixed with translational motion.
- Compared to existing works that employ standalone UWB chips and UWB development boards with full control for prototype implementation, we implement our system on consumer-level smartphones (both iPhone and Android smartphones). Comprehensive experiments are conducted in various environments to show

the effectiveness and robustness of the proposed system. Two real-world applications, i.e., head orientation tracking and 3D reconstruction are developed to showcase the real-world application of orientation estimation.

2 Related Work

Orientation Estimation with Inertial Sensors. In a wide range of real-life scenarios, orientation is as important as location. Conventionally, gyroscopes have been the primary tool for orientation estimation. Recent studies [41, 59, 61] tackled the inherent cumulative errors of gyroscopes by leveraging accelerometers and magnetometers. These methods face challenges when the device is moving or in indoor settings. In contrast, *UWB Orient* provides an orthogonal solution that can achieve highly accurate orientation estimation with smartphone's built-in UWB module.

Orientation Estimation with Wireless Signals. Several systems based on RFID and WiFi have been developed for object orientation tracking [26, 48, 49]. These systems involved the use of multiple RFID tags or a dedicated WiFi card to determine an object's orientation. None of these is available on smartphones. A recent work [22] also proposed an orientation estimation system using GPS signals for drones. Another work [19] leveraged natural sounds in the environment to help determine device's orientation. However, the performance is highly dependent on the sound quality and the coverage is limited. In contrast, *UWB Orient* employs the UWB module that has already been embedded into mainstream smartphones such as iPhone, Samsung, and Pixel phones to achieve accurate orientation estimation.

Orientation Estimation with Cameras. Existing camera-based solutions estimate target orientation via template-matching [24, 42]. Some other works [45] predicted object's poses by implicitly learning from latent space. However, these systems require good lighting and non-occlusion conditions, which may not be met in reality. In contrast, RF signals can penetrate through occlusions and are not limited by lighting conditions.

Fusion of UWB and Inertial Sensor. UWB is popular in localization, which leverages the precise time measurement owing to the large bandwidth [8, 11, 12, 18, 21, 28, 56]. On the other hand, inertial sensors are known for their low cost and wide adoption. Tons of works [7, 16, 25, 34, 57, 58, 60] have utilized inertial sensors for various tracking purposes. A recent work [11] developed a fusion system for precise 2D tracking of pen-like instruments. A fusion system [21] was proposed for cricket ball motion tracking, where UWB handles

localization and IMU measures the spin. An indoor localization system [27] was proposed to fuse UWB ranging and IMU readings. Despite the widely leveraged ranging feature, *UWB Orient* re-purposes the conventional usage and proposes a fusion scheme to combine strengths from both modalities for orientation estimation. To the best of our knowledge, this is the first work fusing UWB and IMU readings on smartphones for orientation estimation.

3 Background

3.1 Orientation v.s. Localization

Orientation and localization refer to distinct aspects of spatial awareness. Localization is the process of determining the target's position in space. On the other hand, orientation refers to the direction in which an object, person, or device is faced or pointed to. In the context of a smartphone, orientation describes how the phone is tilted and in which direction the screen is faced. When a user is using a smartphone (e.g., playing a car racing game), the location of the smartphone may remain unchanged while the orientation can vary significantly. Understanding both is crucial in navigation, robotics, and augmented reality, as they collectively provide a complete picture of an object's placement in the environment [15, 30, 43, 50].

3.2 Inertial-based Orientation Estimation

A gyroscope measures the angular velocity ω_x , ω_y , and ω_z in the object's local frame of x, y, and z axes, respectively. The orientation change (usually represented by a rotation matrix, \mathbf{R}_t^{lf} at timestamp t), can be obtained by integrating the angular velocity on each individual axis from timestamp 0 to timestamp t . The orientation in the global frame, $\langle \text{North}, \text{East}, \text{Up} \rangle$, can be calculated as $\mathbf{R}_t^{gf} = \mathbf{R}_0^{lf \rightarrow gf} \cdot \mathbf{R}_t^{lf}$ once the orientation difference ($\mathbf{R}_0^{lf \rightarrow gf}$) is known.

To address the issue of cumulative errors, prior works corrected the errors by utilizing gravity and magnetic north as reference directions [41, 61]. Specifically, the accelerometer measures the gravity vector when the target is stationary, enabling the determination of the orientation of an object relative to the ground. Concurrently, the magnetometer assesses the target's angle relative to the magnetic north. However, this method requires the target to be stationary for a period of time which can hardly be met when the target keeps moving. The presence of ferromagnetic materials in indoor environments also pollutes the magnetic field readings [44].

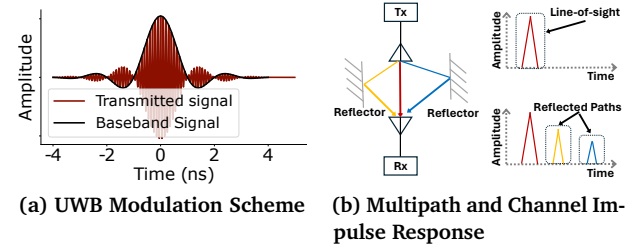


Figure 2: UWB basics (a) A root-raised cosine pulse is modulated. (b) The channel characteristics can be captured.

3.3 Ultra-wideband Radios Basics

Overview. Ultra-wideband (UWB) signal owns a bandwidth larger than 500 MHz or more than 20% of its central carrier frequency [1]. Among several signal types, we focus on the most popular Impulse Radio Ultra-Wideband (IR-UWB),² which modulates signals as short-duration (e.g., 2 ns) pulses. Modern smartphones such as iPhones, Samsung phones, Pixel phones, Mi phones, etc., all employ this short-duration-pulse scheme owing to its simplicity and good performance for ranging. A UWB pulse can be represented as $x(t) = p(t)\cos(2\pi f_c t)$, where $p(t)$ is the baseband pulse and f_c is the carrier frequency. Fig. 2a depicts such signals in the time domain. The receiver may receive multiple copies of the pulse at different timestamps as shown in Fig. 2b, among which the line-of-sight (LoS) path is the shortest.

UWB Information Available on Smartphones. Existing UWB sensing works rely on dedicated UWB hardware or UWB development boards to extract the raw UWB signal amplitude and phase. Unfortunately, the UWB APIs on smartphones [5] can only report the processed distance and angle information. *Distance:* the smartphone API reports the distance between the UWB receiver and transmitter. *Angle:* the smartphone API reports the signal's incident angle information as shown in Fig. 3a. Smartphones such as iPhone and Samsung Galaxy phones can report both azimuth angle and elevation angle.

4 Orientation Estimation with UWB

Now, we present how to obtain fine-grained device orientation estimation using only high-level information (i.e., distance and angle) reported from smartphones.

4.1 Basic Model

4.1.1 Coordinate Transformation. While the obtained high-level information (i.e., distance and angles) from UWB

²In this paper, we use UWB and IR-UWB alternatively for simplicity.

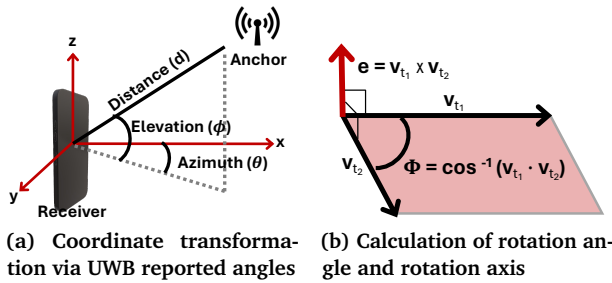


Figure 3: (a) Illustration of UWB reported information and the transformation of Spherical and Cartesian coordinates. Note that the angle information is reported in the receiver's local frame. (b) Illustration of rotation angle and rotational axis, which are essential to describe orientations.

APIs cannot be directly used to describe rotation, the information itself is indeed reported in the spherical coordinate of the device. That said, we can transform the information from spherical to cartesian coordinates as follows. Given the spherical coordinates (d, θ, ϕ) , the Cartesian coordinates (x, y, z) can be calculated as:

$$x = d \cos(\phi) \cos(\theta), y = d \cos(\phi) \sin(\theta), z = d \sin(\phi),$$

where d is the radial distance from the origin, ϕ is elevation angle, and θ is the azimuth angle. Fig. 3a qualitatively describes the transformation. For instance, the radial vector points from the receiver to the transmitter with a length d . Elevation angle ϕ is the angle between the radial vector and its projection onto the x-y plane.

4.1.2 Rotation Matrix Construction. With the coordinate transformation, at any given timestamp t , we can construct a vector v_t in 3D space that points from the signal receiver to the transmitter as follows:

$$v_t = [d \cos(\phi) \cos(\theta), d \cos(\phi) \sin(\theta), d \sin(\phi)]. \quad (1)$$

We further normalize the vector to remove the common factor (i.e., distance d) to obtain the following:

$$v_t = [\cos(\phi) \cos(\theta), \cos(\phi) \sin(\theta), \sin(\phi)]. \quad (2)$$

Next, to describe a rotation from timestamps t_1 to t_2 , we compute the *rotation axis* $e = v_{t_1} \times v_{t_2}$ (\times denotes cross product) and *rotation angle* $\Phi = \cos^{-1}(v_{t_1} \cdot v_{t_2})$, with all vectors normalized. Fig. 3b demonstrates one such example where the rotation axis e is perpendicular to the plane that contains the two vectors (i.e., v_{t_1} and v_{t_2}). Finally, according to Rodrigues' rotation formula [38], the corresponding rotation matrix R that describes the amount of rotation of the device from timestamp t_1 to t_2 can be computed as follows:

$$R = I \cos \Phi + e(e \cdot I)(1 - \cos \Phi) + (e \times I) \sin \Phi, \quad (3)$$

where I is a 3-by-3 identity matrix. We leverage the *Axis-Angle* representation for rotation quantification which exhibits advantages over *Euler Angle* in many aspects such as avoidance of gimbal lock [19, 61]. Based on Eq. 2, we know that the transmitter-device distance does not matter and the orientation estimation depends purely on the angle information. As long as accurate azimuth and elevation angles can be extracted, we can achieve 3D orientation estimation following Eq. 3.

4.2 Interference of Translational Motion

In practice, we hardly see pure rotational motion, and device motion is usually composed of both rotational and translational motions. While the basic model in Sec. 4.1 describes the rotational motion, the translational motion-induced angle is also encapsulated in UWB-reported angles, resulting in inaccurate orientation estimation. However, it is challenging to remove the effect of translational motion with the smartphone-reported high-level distance and angle information because the distance information is relatively coarse (i.e., centimeter-level accuracy) for fine-grained orientation estimation.

In this work, we propose to employ information from the IMU sensor, more specifically, the gyroscope, almost embedded in all smartphones to help address the issues. We believe this is the first time the two sensing modalities are combined on the smartphone owing to the trend of embedding UWB chips into consumer-level devices such as smartphones and smartwatches. Note that IMU sensors alone can not achieve highly accurate orientation estimation either [11, 41, 61]. The gyroscope measures the angular velocities on three axes of the device, which is a completely different sensing modality compared to UWB-based sensing.

5 UWBOrient

In this section, we present the detailed design of *UWBOrient* and the rationale behind the design.

5.1 Comparison of Gyroscope and UWB

To employ a gyroscope to effectively assist UWB-based orientation estimation, we need to understand the characteristics of gyroscope-reported readings on smartphones. As in Sec. 3, gyroscope-based orientation estimation systems are prone to cumulative errors. We conduct experiments to verify this by making the phone stationary facing a fixed direction. Ideally, there should be no angle change over time. However, when we calculate the angle change based on the gyroscope readings after one minute, five minutes, ten minutes, and fifteen minutes, respectively, we can see from Fig. 4b that the gyroscope

error increases over time. In contrast, the UWB-reported angle change is close to 0. To further compare the performance of gyroscope and UWB-based estimates in a short period, we conducted a controlled experiment. Specifically, we fixed the phone onto a step motor as shown in Fig. 4a. We rotated the phone for 20 cycles and repeated the experiment 3 times. Fig. 4c shows that UWB-based estimates are more accurate than those of gyroscope-based even within a short interval (i.e., 20 seconds).

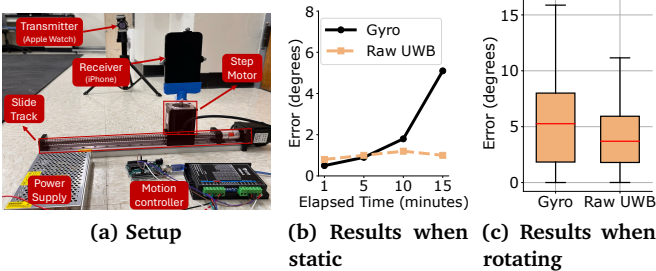


Figure 4: Characterizing the performance of gyroscopes, while comparing with the UWB-based solution. Note that errors of UWB measurements do not accumulate over time and are lower than those of gyroscope-based.

To summarize, we make the observations as follows: (1) The drift issue becomes profound over a long period (i.e., the error accumulates over time), which brings large errors for orientation estimation. However, in a short period (e.g., within a few seconds), the error is still low. (2) The reported UWB angle does not drift over time and is more accurate than gyroscope estimates even in short intervals.

Insights for Fusing Opportunity. To mitigate the effect of translational motion, our key idea is to use the gyroscope estimate as a *reference*. While orientation estimate from the gyroscope drifts over time, ΔR^{Gyro} within a few seconds is accurate. With this reference, we can judge if UWB's estimated orientation is interfered (i.e., contains the translational motion) by comparing ΔR^{UWB} and ΔR^{Gyro} . If they are *roughly equal*, we can trust UWB estimates for orientation estimation because, within this period, UWB estimates are not much affected by translational motion. Otherwise, UWB estimates are interfered with translational motion. With this insight, we can use gyro-readings to assist UWB orientation estimation, mitigating the effect of interfering translational motion.

5.2 Overview

As depicted in Fig. 5, the essence of *UWBOrrient* lies in its innovative multimodal fusion, which we believe is the

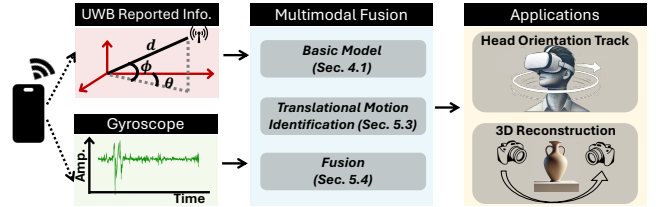


Figure 5: An orientation estimation system based on UWB modules in consumer-level electronics. A multimodal fusion algorithm is proposed to fuse UWB and inertial gyroscopes to efficiently and effectively combine the strengths of both worlds. Accurate estimated orientation is achieved for applications such as head orientation tracking and 3D reconstruction, in which orientations are crucial.

first time UWB and inertial gyroscope in the smartphone are fused for orientation estimation. Our approach results in an effective solution that can be applied to a large number of devices embedded with UWB chips nowadays. In summary, *UWBOrrient* combines the strengths of two sensing modalities, i.e., UWB sensing and IMU sensing on consumer-level devices such as smartphones to deliver precise orientation estimation for applications such as head orientation tracking and 3D reconstruction, in which orientation estimation plays a critical role.

5.3 Identifying Translational Motion

In this section, we propose an identification algorithm that identifies the intervals in which UWB estimates are not reliable, i.e., ΔR^{UWB} is interfered by translational motions. We note that no matter ΔR^{UWB} is interfered or not, ΔR^{Gyro} contains only rotational motion and is accurate over a short period. So we can use ΔR^{Gyro} as a reference to determine if ΔR^{UWB} is interfered. Our solution is to calculate the distance between the two rotation matrices [23]. A threshold is set and if the distance is larger than the threshold, the two rotations are considered different and the UWB estimated orientation is considered interfered. Formally, we can calculate the distance as follows:

$$\begin{aligned} d(\Delta R^{Gyro}, \Delta R^{UWB}) &= (\Delta R^{Gyro})^{-1} \cdot \Delta R^{UWB} - I \\ &= \sum_{i=1}^3 \sum_{j=1}^3 |g_{ij} - I_{ij}|, \end{aligned} \quad (4)$$

where g_{ij} is the elements of $(\Delta R^{Gyro})^{-1} \cdot \Delta R^{UWB}$, and I_{ij} is the elements of identity matrix I . We judge if the UWB estimate is interfered by comparing the distance with an empirical threshold α as follows:

$$\begin{cases} d(\Delta R^{Gyro}, \Delta R^{UWB}) \leq \alpha \rightarrow \text{Not Interfered} \\ d(\Delta R^{Gyro}, \Delta R^{UWB}) > \alpha \rightarrow \text{Interfered} \end{cases} \quad (5)$$

This comparison takes both rotation axis difference and rotation angle difference into account. If UWB estimates are not interfered, we propose to fuse UWB estimates with gyroscope estimates to further increase the accuracy. If UWB estimates are interfered, we replace them with gyroscope estimates and leverage distance information to opportunistically correct the cumulative errors of gyroscope estimates over time.

5.4 Fusing Two Sensing Modalities

Now, we detail the fusion of the two sensing modalities.

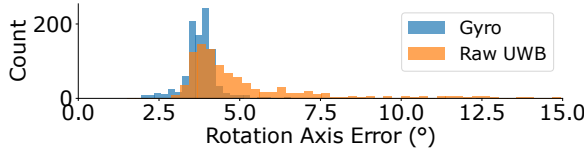


Figure 6: Raw UWB estimates present relatively erroneous rotation axes than that of gyro estimates when comparing against ground truth (y-axis of the phone).

5.4.1 Fusion When UWB Estimates are Not Interfered. When the UWB estimates are not interfered (i.e., small translational motion or pauses between continuous motions), we can directly use UWB estimates for orientation estimation. However, even though gyro estimates are not as accurate as UWB estimates (Section 5.1), they are still relatively accurate in a short interval. As these two sensing modalities are completely different in nature, we propose to fuse them to further improve the orientation estimation accuracy. Our fusion design is motivated by the observation that for UWB estimates, while the rotation angle is more accurate, the rotation axis exhibits larger errors compared to that of gyro estimates. We conducted experiments to rotate a smartphone 1200 times with the help of a step motor to precisely control the amount of rotation. We plot the error for UWB-obtained and gyro-obtained rotation axis respectively. As shown in Fig. 6, we can see that gyro-obtained rotation axis exhibits a smaller error and the error variance is also much smaller. From the experiments, we found that when the rotation angle change is small, larger errors on the rotation axis estimate occur. We believe this is because the rotation axis must be perpendicular to the plane formed by the vector \mathbf{v}_{t_1} and \mathbf{v}_{t_2} in Fig. 3b at the beginning and at the end of the rotation. When the rotation angle change is small, these two vectors also have a small angle difference. In this case, the plane formed by the two vectors can easily be affected by noise and is not that stable, suggesting the same angle error can cause a larger error in the rotation axis.

Based on this observation, we propose to fuse gyro estimates with UWB estimates to combine strengths from both modalities. Specifically, given two rotation matrices obtained from the two modalities, we first calculate their quaternion representations. Then, we fuse them with a weighting parameter $\beta = \frac{1}{2^\Omega}$ (Ω is the angle between UWB estimated and gyro estimated rotation axes) following the method in [31]. Finally, we convert the quaternion back to a rotation matrix. In a nutshell, a varying weight is adopted to dynamically combine UWB estimates and gyro estimates. Formally, the fusion process is expressed as follows:

$$\begin{aligned} \mathbf{q}^{UWB} &= \text{rotm2quaternion}(\Delta\mathbf{R}^{UWB}), \\ \mathbf{q}^{Gyro} &= \text{rotm2quaternion}(\Delta\mathbf{R}^{Gyro}), \\ \mathbf{q}^{Fuse} &= \beta \cdot \mathbf{q}^{UWB} + (1 - \beta) \cdot \mathbf{q}^{Gyro}, \\ \Delta\mathbf{R}^{Fuse} &= \text{quaternion2rotm}(\mathbf{q}^{Fuse}). \end{aligned} \quad (6)$$

Note that Ω is usually small and therefore more weight is still assigned to UWB estimates. We use quaternion for fusion because directly adding two rotation matrices may result in an invalid rotation matrix, i.e., they might not preserve orthogonality and determinant of one [3].

5.4.2 Fusion When UWB Estimates are Interfered. When UWB estimates are interfered, we replace those interfered parts with gyroscope estimates. This yields two more cases. (1) For a relatively short period (e.g., less than two minutes), the accuracy of gyroscope estimates is reasonably high. (2) For a longer period, the drifting issue starts to be profound. To address the large cumulative error (e.g., $> 50^\circ$ [41]) in gyroscope estimates over a long period, we have two key observations: (i) It is rare that a user continuously and translationally moves without any pauses. We notice that even a small pause without translational motion for just 1-2 seconds (i.e., a small not-interfered UWB interval) could be leveraged to address the drifting issue of the gyroscope estimates. (ii) When the receiver (target) is far away from the anchor, the error of orientation estimation caused by the translational motion is not big. To see this, given UWB reported distances (i.e., d_{t_1} and d_{t_2}) at two timestamps t_2 and t_1 , the max angle error caused by interfering translational motion θ^T can be calculated based on the law of cosines as follows:

$$|\theta^T(d_{t_1}, d_{t_2})| \leq \cos^{-1}\left(\frac{(t_2 - t_1)^2 \cdot v^2 - d_{t_1}^2 - d_{t_2}^2}{-2d_{t_1}d_{t_2}}\right), \quad (7)$$

where v is human moving speed, which is usually in the range of 0.8-1.7 m/s for walking. If a receiver is 8 m away from the anchor at t_1 , 8.8 m away from the anchor one second later, and if we assume the human

user moves at a speed lower than 1 m/s, then θ^T is at most 4.1° . In this case, the maximum angle error brought by the translational motion to the orientation estimation is about 6° . In reality, we observe a lot of small pauses and far distances during the usage of smartphones and VR/AR headsets, presenting us with the opportunity to correct the error of gyroscope estimates.

6 Evaluation

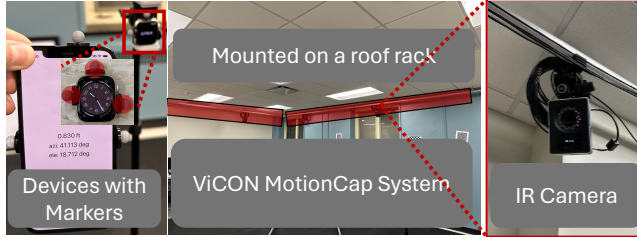


Figure 7: Ground truths are collected by ViCON. Markers are attached to testing devices for ground truths.

6.1 Experiment Setup

■ **Experiment hardware.** We adopt both iPhones (iPhone 12 Pro and iPhone 12) and Android devices including Samsung S21 Ultra and Google Pixel 7 Pro for our experiment. An Apple Smartwatch Series 6 is mainly employed to send out UWB signals as the anchor.

■ **Choice of threshold α .** To detect translational motion, we employed a threshold-based method and empirically set the threshold to 0.04. We employ a single threshold in multiple situations because we use the difference between the UWB-based rotation matrix and the gyroscope-based rotation matrix to determine if there is translational motion. If there is no translational motion, the difference between the two matrices should be quite small and a larger translational motion would induce a larger difference. This difference is thus only dependent on the amount of translational motion, but not the motion type (i.e., walking and running) or the environment.

■ **Baselines.** We compare *UWBOrrient* with four other techniques including two state-of-the-art. **Gyro:** This baseline estimates rotation using a gyroscope via integrating angular velocity over time, with no gravity or magnetometer measurement available for calibration; **Raw UWB:** In this baseline, we use the basic model introduced in Sec. 4.1 without fusing the gyro estimates. **A3 [61]:** A3 estimates 3D orientation using an accelerometer and magnetometer when the device is static. The main principle is to estimate orientation using a gyroscope and opportunistically calibrate the estimation with

the accelerometer and the magnetometer. **MUSE [41]:** MUSE estimates orientation similar to A3 but relies more on the magnetometer for error calibration.

■ **Ground Truth.** We employ a high-end motion capture system ViCON [46] with 8 IR cameras scattered on the roof of a 10 m × 5 m room as shown in Fig. 7 for ground truths. This system can capture an object's location and orientation with errors less than 0.1 mm and 0.5° respectively.

■ **Metrics.** We use *axis-angle error* [17] which is a widely adopted metric to measure the orientation difference between estimated orientations and ground truths [19, 41]. The orientation difference is the minimal angle needed to rotate the estimated orientation to the ground truth. Note that error bars of bar plots denote the standard deviation of n trials in corresponding experiments.

6.2 Evaluation Results

We first compare the performance of *UWBOrrient* on controlled motions with the baselines. We employ controlled motions because they present us with the flexibility to control the rotation angle, rotation axis, and rotation speed for comprehensive evaluation. We also study the performance of *UWBOrrient* under uncontrolled motions. We further study the impact of various factors including distance, multipath, occlusion, anchor orientation, and magnetic interference. We also test our system on different devices to study the generality. Lastly, we study the feasibility of using UWB distance to estimate orientation when UWB reported angles are absent.

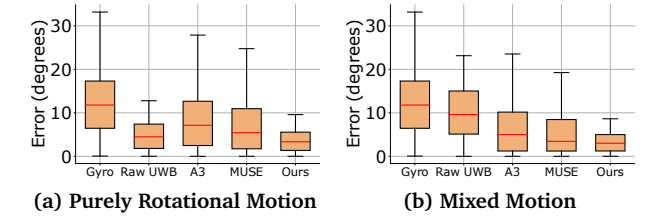


Figure 8: Under different settings, *UWBOrrient* presents stable and accurate estimation.

6.2.1 *Controlled Motion.* To create pure rotational motion, we fix the iPhone on a step motor. For each trial, we rotate the receiver from 0° to 54° counter-clockwise 10 times and clockwise 10 times on a fixed rotation axis (i.e., y-axis). Each trial takes around 1 minute and we repeat the experiments 10 times. The experiment setup is shown in Fig. 4a.

Fig. 8a depicts the experiment results. We can see that *UWBOrrient* performs best with a median error of 3.3° , while other baselines achieve a median error of 11.7° ,

4.4° , 7.1° , and 5.4° , receptively. The large error of *Gyro* is due to the cumulative error over time. While *A3* and *MUSE* improve performance by fusing orientation estimated with gravity and magnetic north readings, the magnetic north can be easily interfered in indoor environments, resulting in high errors. *Raw UWB* is less accurate when the incident angle approaches 90° (Sec. 4.2). *UWBOrient*, on the other hand, takes advantage of the fusing opportunity of accurate gyroscope readings in short intervals to improve the estimates from *Raw UWB*.

We conduct experiments for mixed translational and rotational motions by placing a step motor onto a sliding track. Fig. 8b depicts the results. Evidently, by fusing UWB with gyroscope estimates, *UWBOrient* achieves a median error of 3.0° and a 90%-ile error of 6.9° , which significantly outperforms the state-of-the-art.

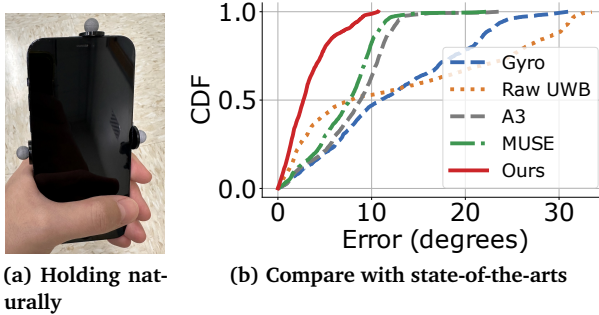


Figure 9: *UWBOrient* outperforms other baselines by a large margin under natural motion setups.

6.2.2 Natural Motion. To study the performance of tracking the orientation of natural motions, we ask a volunteer to naturally hold the smartphone as shown in Fig. 9a. It is worth noting that holding the device naturally by hand does not block the UWB signal. The UWB module is placed near the camera module in the smartphone.

Fig. 9b depicts the orientation error when the smartphone is naturally held by hand and moved freely in the air (i.e., a mixture of translational and rotational motions). Evidently, *UWBOrient*, with a median error of 2.7° , outperforms other baselines (i.e., 10.9° for *Gyro*, 7.7° for *Raw UWB*, 8.8° for *A3*, and 7.6° for *MUSE*) by a large margin. Although gravity readings are polluted under these motions, *MUSE* still relies on the geomagnetic field measurement to correct the drift error in the gyroscope. In contrast, *UWBOrient* dynamically determines whether UWB estimates are interfered, then fuses or replaces the estimates to increase accuracy. On average, *UWBOrient* achieves a significant improvement over *MUSE*.

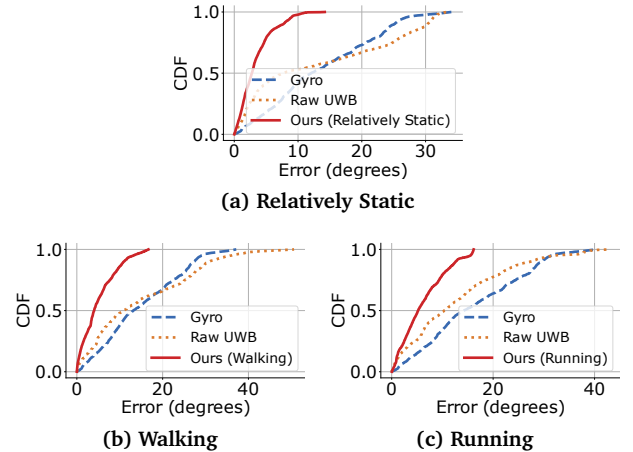


Figure 10: *UWBOrient* is robust to various motion types.

Moreover, we ask the volunteer to rotate their hand arbitrarily while (i) maintaining the location (i.e., keeping the translational motion small), (ii) walking, and (iii) running in the room. Fig. 10 depicts the results. We make two observations as follows. First, the overall performance is accurate and stable, i.e., the median error is $< 5^\circ$ and the max error is $\approx 15^\circ$. Second, the accuracy of either *Gyro* and *Raw UWB* is low. However, *UWBOrient* can dynamically fuse them by alleviating the deficits from both modalities.

6.2.3 Effect of Impact Factors. In this section, we evaluate the effect of various factors including distance, multipath, occlusion, anchor orientation, and magnetic interference on the performance of *UWBOrient*.

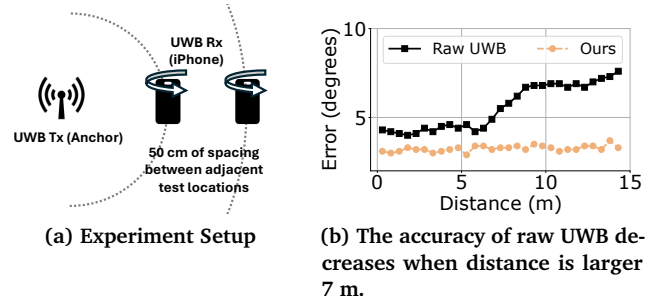


Figure 11: *UWBOrient* adjusts inaccurate raw UWB measurements to achieve a stable error with far distances.

Effect of Distance between Device and Anchor. For a larger distance, the signal gets attenuated more and the orientation estimation error also increases. As illustrated in Fig. 11a, we fix the anchor at one location and increase the distance between the anchor and the receiver smartphone. At each distance, we rotate the

receiver. Fig. 11b depicts the results. When the distance is below 7 m, the error is relatively low (4.3° on average). The error increases to more than 7° when the distance is increased to 9 m for raw UWB. On the other hand, *UWB Orient* yields a lower error ($\approx 3^\circ$) at all distances. We stopped the experiments at 14 m due to the lack of ground truth at further distances.³ We believe the achieved result is promising and encouraging as it presents us with a new modality for highly accurate orientation estimation within a large range in an indoor environment where the geomagnetic field is often interfered and can not be used for precise orientation estimation.

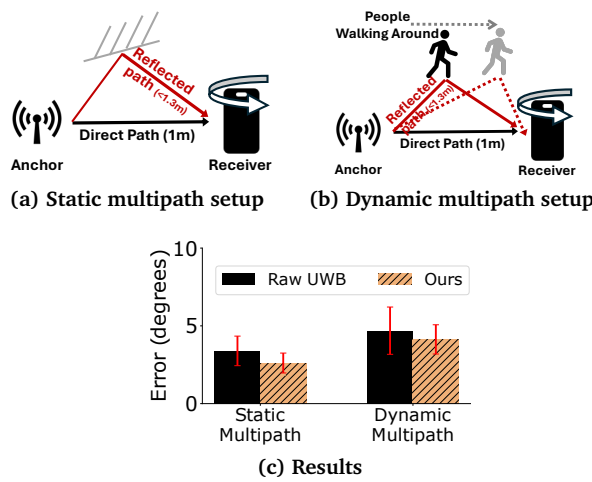


Figure 12: *UWBOrient* is robust to multipaths.

Effect of Static and Dynamic Multipath. First, it is trivial to see that if the multipath from the environment has a long travel distance, UWB estimates will not be affected due to the employment of short-duration pulses (e.g., 2 ns), so the multipath with $> 30\text{cm}$ additional travel distance than the direct path can be filtered out easily. When the additional travel distance is less, we then study the effect of multipath in two groups, i.e., static multipath, and dynamic multipath as shown in Fig. 12a and Fig. 12b. For static multipath, we create a multipath-rich environment by placing hard cardboard around the receiver. For dynamic multipath, we ask a volunteer to walk around. Based on the results in Fig. 12c, we make the following observation. Compared to static multipath which has little effect on the estimation, dynamic multipath can affect the orientation estimation

³Locations at further distances are out of the coverage of the motion capture system used for collecting ground truths.

more because the reported angles vary, resulting in inaccurate orientation. Overall, multipath has a limited effect on *UWB Orient*. Apart from the fine time resolution of the UWB scheme, the duration of such close-by reflected paths in indoor environments would be short. Furthermore, along with our fusion scheme, the effect of multipath can be minimized.

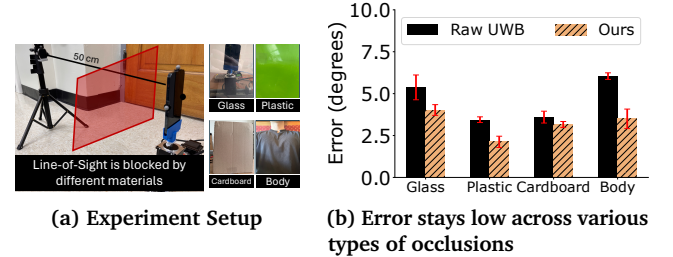


Figure 13: When Line-of-Sight is blocked, UWB radio's quality is affected. Yet, *UWB Orient* adjusts based on these intervals when the reported information is not reliable.

Effect of Non-Line-of-Sight. To study the effect when Non-Line-of-Sight (NLoS) is present, we create an environment as shown in Fig. 13a. Fig. 13b shows the results for four different materials used to block LoS, i.e., glass, plastic, cardboard, and the human body. We make two observations as follows. First, among these materials, the body is the thickest and the signal is not able to penetrate the body. When a volunteer's body blocks LoS, the receiver side reports the signal lost. When the signal is lost, *UWB Orient* replaces the estimates with gyroscope estimates. Fortunately, the duration of this blockage won't be long in practice. Therefore, *UWB Orient* can still maintain a high accuracy. Secondly, other materials cannot block the direct path but the accuracy of the reported angle decreases due to the attenuation of the signal. In contrast to vision-based systems in determining orientations [48, 49], the ability to see through the materials is a plus for *UWB Orient*.

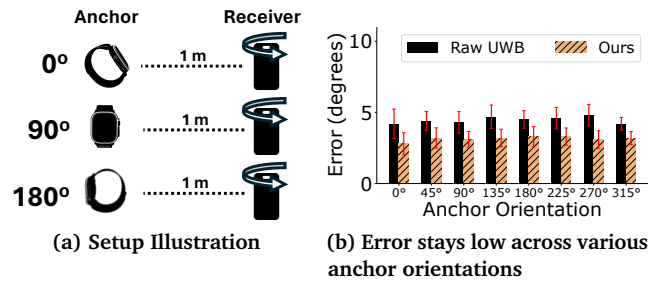


Figure 14: *UWB Orient* is stable across anchor orientations.

Effect of Anchor Orientation. Note that for localization, usually multiple anchors are required. Our system requires only one anchor to work. As we are estimating the target orientation, we would like to study the effect of anchor orientation on the performance of the proposed system. The experiment setup is shown in Fig. 14a. With various anchor orientations, we rotate the receiver (smartphone) 20 cycles at each anchor orientation by a step motor. Fig. 14b shows the error of orientation estimates. We can see that the errors when the anchor faces the receivers are smaller and slightly higher errors are observed otherwise. The overall performance is stable.

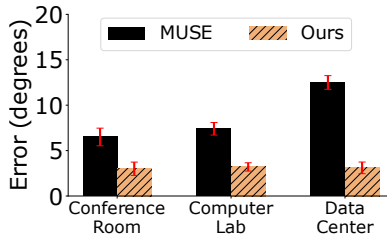


Figure 15: *UWBOrrient* is robust to magnetic interference.

Effect of Magnetic Interference. Lastly, we study the effect of magnetic interference generated by electronics such as smartphones, and computers. We perform experiments with a step motor for precise controls in 1) a conference room, 2) a computer lab, and 3) the room that hosts data servers. Fig. 15 depicts that *UWBOrrient* is significantly better than MUSE [41]. Magnetic fluctuations in these locations lead to larger errors in MUSE because it relies on the magnetometer to correct accumulated errors in gyroscope estimates. In contrast, *UWBOrrient* achieves robust performance in these environments.

To summarize, we demonstrated that *UWBOrrient*'s performance is stable across all these factors. Furthermore, the anchor does not need to be close to the target and the anchor still functions well when it is a few meters away. Next, we validate *UWBOrrient* on various commonly seen platforms in our daily lives.

6.2.4 Performance of *UWBOrrient* on Various Platforms.

Anchor	UWB Receiver
P1	AirTag
P2	Apple Watch S6
P3	iPhone 12
P4	Samsung S21 Ultra
P5	Google Pixel 7 Pro

Table 1: Device setups

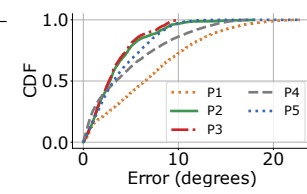


Figure 16: Performance on various device pairs

UWBOrrient leverages the exciting opportunity that consumer-level devices such as smartphones and smartwatches are now equipped with UWB chips. To validate *UWBOrrient*'s performance on various platforms, we conduct experiments on five pairs of devices including AirTag, Apple Watch S6, iPhone 12 pro, Samsung S21 Ultra, and Google Pixel 7 pro as shown in Table 1. We make three observations based on the results depicted in Fig. 16. Firstly, by comparing the performance of AirTag and iPhone (or Apple Watch S6) as transmitters, the dimension of the antenna of UWB transmitters plays an important role. The size and design of the antenna can impact its radiation efficiency. Secondly, Apple devices perform slightly better than Androids. Lastly, although a single AirTag achieves slightly larger errors, it is easy to extend *UWBOrrient* with multiple AirTags (each is \$25 with a year-long battery life) as anchors to address issues such as out-of-field-of-view. In a nutshell, *UWBOrrient* achieves decent accuracy on these commodity devices without a need of any modification. The anchors can be randomly and flexibly placed, suggesting the flexibility of *UWBOrrient*.

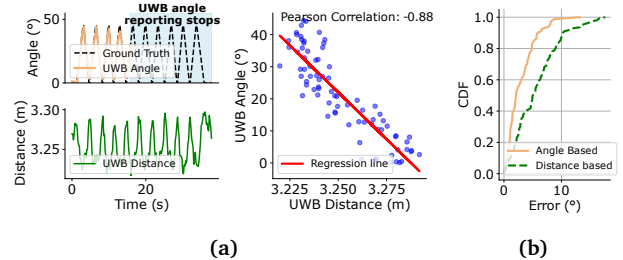


Figure 17: (a) When UWB APIs stop reporting UWB angles within the shaded area, *UWBOrrient* explores the highly correlated UWB distance in rotational motion to estimate angles. (b) In contrast to unbounded errors, the UWB distance estimated angle is reasonable, extending the continuity of *UWBOrrient* in orientation estimation.

6.2.5 Study of UWB distance based Angle Estimation. when the smartphone API stops reporting UWB angles, we estimate the orientation based on UWB-reported distance in Sec. 6.2.5. We find that when the receiver is rotating, UWB-reported distance is highly correlated with the receiver's rotation motion as shown in Fig. 17a. We further study if we can employ the reported distance information for angle estimation. Based on Fig. 17a (right), we can see that the UWB distance is correlated with the UWB angle. We show the angle estimation errors based on UWB distance and angle readings respectively in Fig. 17b. We can see that although the accuracy of UWB-distance-based angle estimation is lower than UWB-angle-based

estimation, it is still relatively accurate which can be used to ensure *UWBOrrient*'s continuity for orientation estimation when UWB-reported angles are not available (e.g., UWB API stops reporting angle readings when the angle is large).

6.3 Latency and Energy Consumption

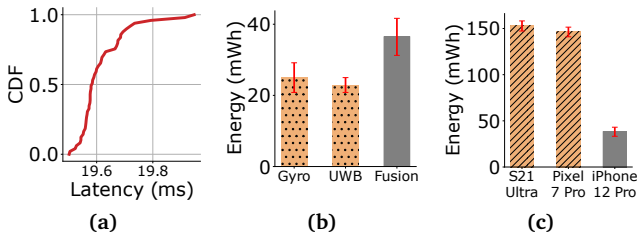


Figure 18: (a) *UWBOrrient*'s latency is sufficient for real-time operation. (b)(c) energy consumption across various modalities (with iPhone 12 Pro) and devices demonstrates that fusion is energy efficient. Note that the gray bars denote the same data.

Note that if *UWBOrrient* processes UWB-reported data every 18 ms (i.e., UWB reporting rate is 55 Hz), a relatively large error can be observed. To balance off the latency and the accuracy, we adjust *UWBOrrient* to process a chunk of reported data every 180 ms. To further optimize, we make a modification that at any given instant of time, the previously reported partial data are again used to obtain instantaneous real-time results. With this modification, *UWBOrrient* only incurs a delay of 180 ms once in the beginning. As shown in Fig. 18a, the system latency is less than 20 ms, which is sufficient for real-time purposes. The UWB reporting rate restricts the latency of our system, and the signal processing time is quite low due to small-size matrix multiplication, which is optimized on modern processors [6]. In a nutshell, *UWBOrrient*'s latency is comparable to the motion-to-photon latency (i.e., the lag between user action and system response) in modern VR/AR systems.

To study the energy consumption, we measure the energy consumption when the receiver (iPhone 12 Pro) continuously collects UWB signals and/or gyroscope data for one hour with the help of corresponding developer tools (e.g., Xcode for iPhones). Fig. 18b depicts the energy consumption when different types of data are collected. UWB consumes less energy while Gyro consumes more energy due to the higher sampling rate. We do not observe a dramatic increase in energy consumption for the fusion case, suggesting *UWBOrrient* inherits the low-energy nature of the two modalities. Fig. 18c

shows the overall energy consumption of the fusion operation on different devices, i.e., ≈ 150 mWh on Android smartphones and ≈ 37 mWh on iPhones respectively. The difference across platforms might be caused by the different energy management strategies. In short, the energy consumption of UWB modules embedded in smartphones is quite low, suggesting the energy consumption of *UWBOrrient* is not an issue for smartphones.

6.4 Application Study

To showcase the application of *UWBOrrient* in the real world, we apply the proposed orientation estimation system to realize two representative applications, i.e., head orientation tracking and 3D reconstruction.

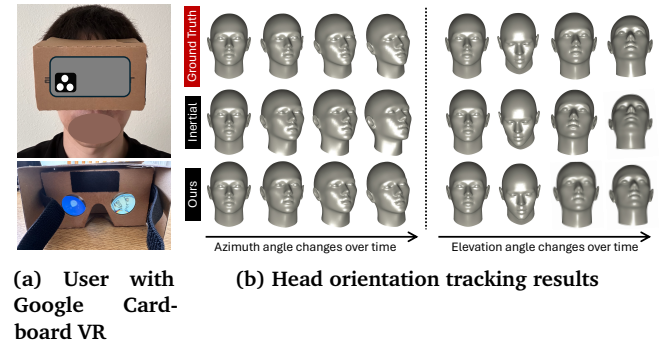


Figure 19: *UWBOrrient*'s tracking error stays low compared to that of inertial-based systems. Better orientation estimations provide a better immersive experience.

6.4.1 Head Orientation Tracking. Head orientation estimation plays a pivotal role in virtual reality (VR) and augmented reality (AR), as continuously tracking the user's head orientation is crucial for creating an immersive and interactive environment [30, 50]. To this end, we conduct experiments to showcase *UWBOrrient*'s performance in tracking users' head orientation. In the experiment, we track the rotation angle of two typical head motions (i.e., left-to-right: azimuth angle; and up-to-down: elevation angle).⁴ In AR/VR, these two basic motions are important because they provide critical information for VR/AR systems to infer the focus of the user. We asked a volunteer to wear a Google Cardboard VR with iPhone 12 Pro mounted in it as shown in Fig. 19a, and the volunteer rotated the head from left to right and up to down multiple times. Fig. 19b qualitatively depicts the tracking results. The inertial-based system suffers from drifting

⁴We skip right-to-left here as it is the same as left-to-right in terms of tracking performance.

issues with an average error of 8° . In contrast, *UWBOrbit*'s tracking performance is closer to the ground truth with an average error of 3° . With more attention on VR/AR from leading companies such as Apple, Meta, and Samsung, wireless-based orientation sensing, as an alternative demonstrated by *UWBOrbit*, is promising.

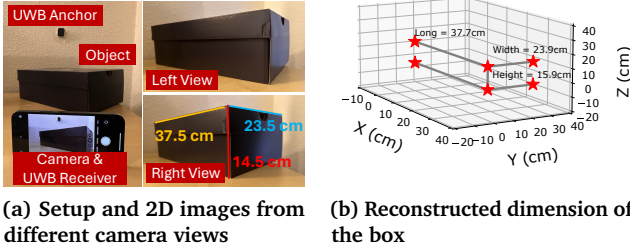


Figure 20: *UWBOrbit* reconstructs the dimension of the object from two 2D images at different camera views.

6.4.2 3D Reconstruction. 3D reconstruction is widely used in diverse real-life applications such as virtual reality and arts reconstruction [20, 51]. To reconstruct an object in 3D, multiple images need to be taken at different orientations. Therefore, a small orientation deviation can lead to large 3D reconstruction errors. We demonstrate that *UWBOrbit* can help reconstruct 3D objects accurately. Fig. 20a shows two photos of an object (i.e., a box) from different views, with which the dimension of the box can be calculated based on the known camera's parameters (focal length, etc.), and orientations obtained from *UWBOrbit* at different views [35]. Fig. 20b depicts the 3D dimensions of the reconstructed box. Owing to the highly accurate orientation estimates, the box is reconstructed highly accurately with a small average error of 3.9% compared to the ground truth dimensions.

7 Discussion

Multi-Anchor Deployment. As demonstrated in Sec. 6, the anchor of *UWBOrbit* can be randomly and flexibly placed, and commonly seen AirTags and phones can be used as anchors. This presents us the opportunity to deploy multiple anchors at low cost with several benefits: 1) *UWBOrbit*'s coverage can be further extended with multiple anchors. 2) *UWBOrbit* could utilize the reported angles from multiple anchors to retain the estimation accuracy in case the angles are large and some UWB modules start to report inaccurate angles.

Potential Applications. Fine orientation estimation plays an important role in 3D games, VR/AR, etc. Besides dedicated VR/AR headsets, smartphones such as

Samsung Galaxy phones can also be used with Galaxy Gear or Google Cardboard VR to become a VR platform. As more manufacturers integrate UWB modules into everyday devices, we believe UWB-based orientation estimation can support a wide range of applications and this work makes the first attempt in this direction.

Mobility removal. As incorporating UWB chips in consumer-level devices becomes more and more popular, no extra hardware requirement is a big plus to bring wireless sensing to the general public. Traditional wireless sensing requires devices to be static, which is not realistic for consumer-level devices such as smartphones. Therefore, removing the mobility of the device is critical if we want to push wireless sensing for real-life adoption [55]. As one important mobility type, rotation motion needs to be accurately measured before the effect of rotation motion on sensing can be removed.

Potential usage of low-level UWB information. Currently, smartphone manufacturers are not reporting low-level UWB signal information such as amplitude and phase possibly due to the large volume of raw UWB signal samples and security concerns. We thus believe leveraging the high-level UWB readings (i.e., distance and angle) for sensing has great significance. We do believe the performance of *UWBOrbit* can be further improved if low-level data is available in the future. 1) While the high-level data only reports the distance/angle information of the first path, low-level data contains the information of all the paths. By utilizing information from multiple paths, it is possible to remove the translational motion without the need of IMU. 2) With information reported from multiple range bins instead of just the first range bin, multi-target sensing becomes possible.

8 Conclusion

We propose *UWBOrbit*, the first orientation estimation system that utilizes UWB modules in electronics such as smartphones. It introduces a multimodal fusion scheme that combines the strengths of UWB radios and gyroscopes. *UWBOrbit* effectively deals with issues like mixed motions, and multipath. The system achieves a low median error of 2.7° . The efficacy and practicality of *UWBOrbit* are verified through extensive real-life experiments and representative applications.

Acknowledgements

Our gratitude goes to the anonymous reviewers and shepherds for their invaluable feedback.

References

- [1] 2024. FCC Regulation On UWB. <https://www.ecfr.gov/current/title-47/chapter-I/subchapter-A/part-15/subpart-F>.
- [2] Fadel Adib and Dina Katabi. 2013. See through walls with WiFi!. In *Proceedings of the ACM SIGCOMM 2013 conference on SIGCOMM*. 75–86.
- [3] Tomas Akenine-Moller, Eric Haines, and Naty Hoffman. 2019. *Real-time rendering*. AK Peters/crc Press.
- [4] Apple Find My 2024. One app to find it all. <https://www.apple.com/icloud/find-my/>.
- [5] Apple Nearby Interaction 2024. Apple Nearby Interaction. <https://developer.apple.com/nearby-interaction/>.
- [6] Apple SIMD 2021. Perform computations on small vectors and matrices. <https://developer.apple.com/documentation/accelerate/simd>.
- [7] Rayan Armani, Changlin Qian, Jiaxi Jiang, and Christian Holz. 2024. Ultra inertial poser: Scalable motion capture and tracking from sparse inertial sensors and ultra-wideband ranging. In *ACM SIGGRAPH 2024 Conference Papers*. 1–11.
- [8] Aditya Arun, Shunsuke Saruwatari, Sureel Shah, and Dinesh Bharadia. 2023. XRLoc: Accurate UWB Localization to Realize XR Deployments. (2023).
- [9] BMW Keyless Entry 2024. All you need to know about Ultra Wideband tech. <https://www.bmw.com/en/innovation/bmw-digital-key-plus-ultra-wideband.html>.
- [10] Gaoshuai Cao, Kuang Yuan, Jie Xiong, Panlong Yang, Yubo Yan, Hao Zhou, and Xiang-Yang Li. 2020. Earphonetrack: involving earphones into the ecosystem of acoustic motion tracking. In *Proceedings of the 18th Conference on Embedded Networked Sensor Systems*. 95–108.
- [11] Yifeng Cao, Ashutosh Dhekne, and Mostafa Ammar. 2021. ITrackU: tracking a pen-like instrument via UWB-IMU fusion. In *Proceedings of the 19th Annual International Conference on Mobile Systems, Applications, and Services*. 453–466.
- [12] Yifeng Cao, Ashutosh Dhekne, and Mostafa Ammar. 2023. Visig: Automatic interpretation of visual body signals using on-body sensors. *Proceedings of the ACM on Interactive, Mobile, Wearable and Ubiquitous Technologies* 7, 1 (2023), 1–27.
- [13] Yifeng Cao, Ashutosh Dhekne, and Mostafa Ammar. 2024. UTrack3D: 3D Tracking Using Ultra-wideband (UWB) Radios. In *Proceedings of the 22nd Annual International Conference on Mobile Systems, Applications and Services*. 345–358.
- [14] Haige Chen and Ashutosh Dhekne. 2022. Pnploc: Uwb based plug & play indoor localization. In *2022 IEEE 12th International Conference on Indoor Positioning and Indoor Navigation (IPIN)*. IEEE, 1–8.
- [15] Xinke Deng, Yu Xiang, Arsalan Mousavian, Clemens Eppner, Timothy Bretl, and Dieter Fox. 2020. Self-supervised 6d object pose estimation for robot manipulation. In *2020 IEEE International Conference on Robotics and Automation (ICRA)*. IEEE, 3665–3671.
- [16] Nathan DeVrio, Vimal Mollyn, and Chris Harrison. 2023. SmartPoser: Arm Pose Estimation with a Smartphone and Smartwatch Using UWB and IMU Data. In *Proceedings of the 36th Annual ACM Symposium on User Interface Software and Technology*. 1–11.
- [17] James Diebel et al. 2006. Representing attitude: Euler angles, unit quaternions, and rotation vectors. *Matrix* 58, 15–16 (2006), 1–35.
- [18] Daquan Feng, Chunqi Wang, Chunlong He, Yuan Zhuang, and Xiang-Gen Xia. 2020. Kalman-filter-based integration of IMU and UWB for high-accuracy indoor positioning and navigation. *IEEE Internet of Things Journal* 7, 4 (2020), 3133–3146.
- [19] Zhihui Gao, Ang Li, Dong Li, Jialin Liu, Jie Xiong, Yu Wang, Bing Li, and Yiran Chen. 2022. Mom: Microphone based 3d orientation measurement. In *2022 21st ACM/IEEE International Conference on Information Processing in Sensor Networks (IPSN)*. IEEE, 132–144.
- [20] Leonardo Gomes, Olga Regina Pereira Bellon, and Luciano Silva. 2014. 3D reconstruction methods for digital preservation of cultural heritage: A survey. *Pattern Recognition Letters* 50 (2014), 3–14.
- [21] Mahanth Gowda, Ashutosh Dhekne, Sheng Shen, Romit Roy Choudhury, Lei Yang, Suresh Golwalkar, and Alexander Essanian. 2017. Bringing {IoT} to sports analytics. In *14th USENIX Symposium on Networked Systems Design and Implementation (NSDI 17)*. 499–513.
- [22] Mahanth Gowda, Justin Manweiler, Ashutosh Dhekne, Romit Roy Choudhury, and Justin D Weisz. 2016. Tracking drone orientation with multiple GPS receivers. In *Proceedings of the 22nd annual international conference on mobile computing and networking*. 280–293.
- [23] Arthur Gretton, Olivier Bousquet, Alex Smola, and Bernhard Schölkopf. 2005. Measuring statistical dependence with Hilbert-Schmidt norms. In *International conference on algorithmic learning theory*. Springer, 63–77.
- [24] Stefan Hinterstoisser, Vincent Lepetit, Slobodan Ilic, Pascal Fua, and Nassir Navab. 2010. Dominant orientation templates for real-time detection of texture-less objects. In *2010 IEEE Computer Society Conference on Computer Vision and Pattern Recognition*. IEEE, 2257–2264.
- [25] Yinghao Huang, Manuel Kaufmann, Emre Aksan, Michael J Black, Otmar Hilliges, and Gerard Pons-Moll. 2018. Deep inertial poser: Learning to reconstruct human pose from sparse inertial measurements in real time. *ACM Transactions on Graphics (TOG)* 37, 6 (2018), 1–15.
- [26] Chengkun Jiang, Yuan He, Xiaolong Zheng, and Yunhao Liu. 2018. Orientation-aware RFID tracking with centimeter-level accuracy. In *2018 17th ACM/IEEE International Conference on Information Processing in Sensor Networks (IPSN)*. IEEE, 290–301.
- [27] Fan Jiang, David Caruso, Ashutosh Dhekne, Qi Qu, Jakob Julian Engel, and Jing Dong. 2023. Robust Indoor Localization with Ranging-IMU Fusion. *arXiv preprint arXiv:2309.08803* (2023).
- [28] Benjamin Kempke, Pat Pannuto, and Prabal Dutta. 2016. Harmonium: Asymmetric, bandstitched UWB for fast, accurate, and robust indoor localization. In *2016 15th ACM/IEEE International Conference on Information Processing in Sensor Networks (IPSN)*. IEEE, 1–12.
- [29] Dong Li, Jialin Liu, Sunghoon Ivan Lee, and Jie Xiong. 2020. FM-track: pushing the limits of contactless multi-target tracking using acoustic signals. In *Proceedings of the 18th Conference on Embedded Networked Sensor Systems*. 150–163.
- [30] Jiaman Li, Karen Liu, and Jiajun Wu. 2023. Ego-Body Pose Estimation via Ego-Head Pose Estimation. In *Proceedings of the IEEE/CVF Conference on Computer Vision and Pattern Recognition*. 17142–17151.
- [31] Zhiyuan Li and Sanjeev Arora. 2019. An exponential learning rate schedule for deep learning. *arXiv preprint arXiv:1910.07454* (2019).
- [32] Wenguang Mao, Jian He, and Lili Qiu. 2016. Cat: high-precision acoustic motion tracking. In *Proceedings of the 22nd Annual International Conference on Mobile Computing and Networking*. 69–81.

- [33] Wenguang Mao, Mei Wang, and Lili Qiu. 2018. Aim: Acoustic imaging on a mobile. In *Proceedings of the 16th Annual International Conference on Mobile Systems, Applications, and Services*. 468–481.
- [34] Vimal Mollyn, Riku Arakawa, Mayank Goel, Chris Harrison, and Karan Ahuja. 2023. Imuposer: Full-body pose estimation using imus in phones, watches, and earbuds. In *Proceedings of the 2023 CHI Conference on Human Factors in Computing Systems*. 1–12.
- [35] Theo Moons, Luc Van Gool, Maarten Vergauwen, et al. 2010. 3D reconstruction from multiple images part 1: Principles. *Foundations and Trends® in Computer Graphics and Vision* 4, 4 (2010), 287–404.
- [36] Point-to-Point 2024. Xiaomi Introduces groundbreaking UWB Technology. <https://www.mi.com/global/discover/article?id=2287>.
- [37] Anshul Rai, Krishna Kant Chintalapudi, Venkata N Padmanabhan, and Rijurekha Sen. 2012. Zee: Zero-effort crowdsourcing for indoor localization. In *Proceedings of the 18th annual international conference on Mobile computing and networking*. 293–304.
- [38] Olinde Rodrigues. 1840. Des lois géométriques qui régissent les déplacements d'un système solide dans l'espace, et de la variation des coordonnées provenant de ces déplacements considérés indépendamment des causes qui peuvent les produire. *Journal de mathématiques pures et appliquées* 5 (1840), 380–440.
- [39] Samsung Phones 2024. What is UWB in the Galaxy S21 series and which models support it? <https://www.androidcentral.com/what-uwb-galaxy-s21-series-and-which-models-support-it>.
- [40] Guobin Shen, Zhuo Chen, Peichao Zhang, Thomas Moscibroda, and Yongguang Zhang. 2013. {Walkie-Markie}: indoor pathway mapping made easy. In *10th USENIX Symposium on Networked Systems Design and Implementation (NSDI 13)*. 85–98.
- [41] Sheng Shen, Mahanth Gowda, and Romit Roy Choudhury. 2018. Closing the gaps in inertial motion tracking. In *Proceedings of the 24th Annual International Conference on Mobile Computing and Networking*. 429–444.
- [42] Yujiao Shi, Xin Yu, Dylan Campbell, and Hongdong Li. 2020. Where am i looking at? joint location and orientation estimation by cross-view matching. In *Proceedings of the IEEE/CVF Conference on Computer Vision and Pattern Recognition*. 4064–4072.
- [43] Mohit Shridhar, Lucas Manuelli, and Dieter Fox. 2023. Perceiver-actor: A multi-task transformer for robotic manipulation. In *Conference on Robot Learning*. PMLR, 785–799.
- [44] Yuanchao Shu, Cheng Bo, Guobin Shen, Chunshui Zhao, Liqun Li, and Feng Zhao. 2015. Magicol: Indoor localization using pervasive magnetic field and opportunistic WiFi sensing. *IEEE Journal on Selected Areas in Communications* 33, 7 (2015), 1443–1457.
- [45] Martin Sundermeyer, Zoltan-Csaba Marton, Maximilian Durner, Manuel Brucker, and Rudolph Triebel. 2018. Implicit 3d orientation learning for 6d object detection from rgb images. In *Proceedings of the european conference on computer vision (ECCV)*. 699–715.
- [46] ViCON 2024. Motion Capture System. <https://www.vicon.com/>.
- [47] He Wang, Souvik Sen, Ahmed Elgohary, Moustafa Farid, Moustafa Youssef, and Romit Roy Choudhury. 2012. No need to war-drive: Unsupervised indoor localization. In *Proceedings of the 10th international conference on Mobile systems, applications, and services*. 197–210.
- [48] Teng Wei and Xinyu Zhang. 2016. Gyro in the air: tracking 3d orientation of batteryless internet-of-things. In *Proceedings of the 22nd Annual International Conference on Mobile Computing and Networking*. 55–68.
- [49] Chenshu Wu, Feng Zhang, Yusen Fan, and KJ Ray Liu. 2019. RF-based inertial measurement. In *Proceedings of the ACM Special Interest Group on Data Communication*. 117–129.
- [50] Min-Yu Wu, Pai-Wen Ting, Ya-Hui Tang, En-Te Chou, and Li-Chen Fu. 2020. Hand pose estimation in object-interaction based on deep learning for virtual reality applications. *Journal of Visual Communication and Image Representation* 70 (2020), 102802.
- [51] Haozhe Xie, Hongxun Yao, Xiaoshuai Sun, Shangchen Zhou, and Shengping Zhang. 2019. Pix2vox: Context-aware 3d reconstruction from single and multi-view images. In *Proceedings of the IEEE/CVF international conference on computer vision*. 2690–2698.
- [52] Yaxiong Xie, Jie Xiong, Mo Li, and Kyle Jamieson. 2019. mD-Track: Leveraging multi-dimensionality for passive indoor Wi-Fi tracking. In *The 25th Annual International Conference on Mobile Computing and Networking*. 1–16.
- [53] Jie Xiong and Kyle Jamieson. 2013. {ArrayTrack}: A {Fine-Grained} indoor location system. In *10th USENIX Symposium on Networked Systems Design and Implementation (NSDI 13)*. 71–84.
- [54] Fusang Zhang, Zhaoxin Chang, Jie Xiong, Junqi Ma, Jiazhi Ni, Wenbo Zhang, Beihong Jin, and Daqing Zhang. 2023. Embracing Consumer-level UWB-equipped Devices for Fine-grained Wireless Sensing. *Proceedings of the ACM on Interactive, Mobile, Wearable and Ubiquitous Technologies* 6, 4 (2023), 1–27.
- [55] Fusang Zhang, Jie Xiong, Zhaoxin Chang, Junqi Ma, and Daqing Zhang. 2022. Mobi2Sense: empowering wireless sensing with mobility. In *Proceedings of the 28th Annual International Conference on Mobile Computing And Networking*. 268–281.
- [56] Minghui Zhao, Tyler Chang, Aditya Arun, Roshan Ayyalasomayajula, Chi Zhang, and Dinesh Bharadia. 2021. Uloc: Low-power, scalable and cm-accurate uwb-tag localization and tracking for indoor applications. *Proceedings of the ACM on Interactive, Mobile, Wearable and Ubiquitous Technologies* 5, 3 (2021), 1–31.
- [57] Hao Zhou, Taiting Lu, Kenneth DeHaan, and Mahanth Gowda. 2024. ASLRing: American Sign Language Recognition with Meta-Learning on Wearables. In *2024 IEEE/ACM Ninth International Conference on Internet-of-Things Design and Implementation (IoTDI)*. IEEE, 203–214.
- [58] Hao Zhou, Taiting Lu, Yilin Liu, Shijia Zhang, and Mahanth Gowda. 2022. Learning on the Rings: Self-Supervised 3D Finger Motion Tracking Using Wearable Sensors. *Proceedings of the ACM on Interactive, Mobile, Wearable and Ubiquitous Technologies* 6, 2 (2022), 1–31.
- [59] Hao Zhou, Taiting Lu, Yilin Liu, Shijia Zhang, Runze Liu, and Mahanth Gowda. 2023. One Ring to Rule Them All: An Open Source Smartring Platform for Finger Motion Analytics and Healthcare Applications. In *Proceedings of the 8th ACM/IEEE Conference on Internet of Things Design and Implementation*. 27–38.
- [60] Hao Zhou, Taiting Lu, Kristina Mckinnie, Joseph Palagano, Kenneth Dehaan, and Mahanth Gowda. 2023. SignQuery: A Natural User Interface and Search Engine for Sign Languages with Wearable Sensors. In *Proceedings of the 29th Annual International Conference on Mobile Computing and Networking*. 1–16.
- [61] Pengfei Zhou, Mo Li, and Guobin Shen. 2014. Use it free: Instantly knowing your phone attitude. In *Proceedings of the 20th annual international conference on Mobile computing and networking*. 605–616.